Reducing PM$_{2.5}$ and O$_3$ through optimizing urban ecological land form based on its size thresholds

Xin Chen [*], Fang Wei

College of Civil Engineering and Architecture, Zhejiang University, Hangzhou, 310058, China

ARTICLE INFO

ABSTRACT

Optimizing the size and form of urban ecological land (UEL) is an effective approach to addressing PM$_{2.5}$-O$_3$ composite pollution in China. However, existing strategies are usually proposed based on the impact of one type of UEL on individual pollutants, while overlooking UEL forms' different pollution reduction effects across its size intervals. This study identifies UELs (including forest, shrub, grassland, water, and wetland) of 1068 counties within the Yangtze River Economic Belt (YREB) and calculates their size and form metrics. Then the cross-sectional threshold regression model is used to analyze the threshold effect of UEL size on fitting models of pollutant concentrations. Finally, quadrant analysis is extended to categorize counties and provide differentiated planning strategies. The conclusions show: (1) UEL size presents a triple threshold effect on PM$_{2.5}$ concentrations at 4.302%, 8.055%, and 23.742%, and a single threshold effect on O$_3$ concentrations at 3.275%. Size and form metrics are not always significant across UEL size intervals. (2) Counties are categorized into 6 types based on their primary pollutants and UEL sizes, showing spatial clustering within each type. (3) With size increasing, dispersed and irregular UEL form helps more in reducing PM$_{2.5}$, while O$_3$ reduction prefers aggregated one, thereby the evolutionary UEL planning strategy is proposed.

1. Introduction

PM$_{2.5}$ and O$_3$ have become the primary air pollutants in China (Wu et al., 2024; Yang et al., 2023), posing risks to ecological balance, public health, and socio-economic development (Guan et al., 2021; Knippertz et al., 2015; Zhang et al., 2022). Given that urban space is the central hub of human activity (Li et al., 2021), efforts must be taken to address PM$_{2.5}$-O$_3$ composite pollution within it. Land serves as the primary carrier of anthropogenic pollutant emission sources (Wu et al., 2021), influences the spatial distribution of pollutants by acting as an atmospheric substrate (Lu et al., 2018), and regulates the local microclimate through spatial pattern adjustments (Wang et al., 2018). Therefore, optimizing spatial patterns of various land types is recognized as an effective strategy for improving air quality (Li et al., 2022; Lu et al., 2020).

Among different land types, urban ecological land (UEL) includes natural and semi-natural ecosystems within the city, comprising vegetation (belonging to forest, grassland, etc., considered green spaces) and water bodies (belonging to water, wetland, etc., considered blue spaces) (Chen et al., 2014; Feng et al., 2021; Hunter et al., 2019). UEL provides ecological, economic, and social services, making it a vital land type in atmospheric governance and urban planning (Gómez-Baggethun and Barton, 2013; Zhang et al., 2021). Size and form are two key factors in land planning research and practice (Mo et al., 2019; Shih, 2017). Size refers to the area of land use, represented by its proportion of the total land area. Form pertains to the spatial geometric characteristics of the land, such as shape regularity and patch aggregation (Lu et al., 2020; Yang et al., 2022). Effective pollution reduction can only be achieved by properly optimizing both the size and form of UEL.

Existing research has explored the impact of UEL on PM$_{2.5}$/O$_3$ from the perspectives of size and form separately, while also acknowledging the matching relationship between size and form. For example, regarding the independent roles of size or form, urban green spaces can adsorb and degrade particulate matter, with greater effectiveness when their area is larger and aggregation is higher (Cai et al., 2020; Fan et al., 2022). Urban lakes and wetlands can reduce PM$_{2.5}$ by increasing local humidity and enhancing surrounding wind speed, with the effect positively correlated to both their area and shape complexity (Liu et al., 2018a; Zhu and Zeng, 2018). Vegetation within green spaces can release ozone precursors, with this effect being more pronounced in continuous

---

and densely vegetated areas (Cai et al., 2022; Han et al., 2024). Regarding the matching between UEL size and form, Quattrochi and Pelletier proposed that urban green space form provides the greatest ecological benefits when the area coverage is less than 40% (Bi et al., 2022; Lin et al., 2024); Zhu and Zeng (2018) found that for lake wetlands with area smaller than 0.2 km^2, greater shape complexity was negatively correlated with PM$_{2.5}$ concentrations. However, green and blue spaces are intricately interwoven within urban environments (Feng et al., 2021; Hu et al., 2020a). Integrating them as UEL facilitates a more comprehensive understanding of their synergistic effects and aligns more closely with reality (Peng et al., 2016; Wang et al., 2023c). Therefore, the impacts of UEL (a whole integrating all types) size and form on different pollutants require further investigation.

Some studies have identified the threshold effects of UEL size on pollutant concentrations (Liu et al., 2018b; Yu et al., 2020). Specifically, the unit ecological effects (including reducing pollution) of UEL experience significant shifts once UEL size exceeds a specific threshold (Fan et al., 2019; Peng et al., 2016). For example, Zhou et al. (2019) found that forests are more effective at reducing PM$_{2.5}$ when their coverage surpasses 30% within urban space. To investigate the threshold effects of UEL size on its ecological benefits, methods of two types are mainly used: (1) parameterized nonlinear regression models, such as polynomial regression, quantile regression, and piecewise regressions (Liu et al., 2018b; Zhao and Zhang, 2024; Zhao et al., 2024); and (2) non-parameterized nonlinear fitting mapping methods, such as partial dependence plots from machine learning models (e.g., random forests, eXtreme Gradient Boosting) (Han et al., 2022; Li et al., 2023; Zhu et al., 2024). Among these methods, the non-parametric plotting does not yield a fitted formula, and the threshold effect of a given factor can only be observed graphically. Meanwhile, most parametric regression models reveal the threshold effect of UEL size itself, without providing insights into its effects on other factors. However, as mentioned earlier, there is a suitable matching between UEL form and size. Considering the difficulty of adjusting UEL size to its optimal value in reality (Liu and Zhou, 2021), understanding the impact of UEL form on pollutants across UE size intervals can inform targeted optimization strategies. Therefore, it is crucial to select appropriate methods to analyze the threshold effects of UEL size on correlations between UF form and pollutant concentrations.

The Yangtze River Economic Belt (YREB) is a major region in China, characterized by a similar climate but diverse geographical conditions and varying pollution levels. To fill the research gaps, this study identified the ecological lands and air pollutant status in urban spaces of 1068 counties within the YREB. Subsequently, the cross-sectional threshold regression model was applied to analyze the threshold effect of UEL size on pollutant concentrations, as well as the pollution reduction effects of UEL form at different size intervals. Lastly, this study extended the quadrant analysis to categorize counties based on their

primary pollutants and UEL sizes. The marginal contributions of this study lie in (1) targeting PM$_{2.5}$ and O$_3$ as the pollutants and treating all types of UEL as a whole, which provides better alignment with atmospheric governance and urban planning. (2) This study fully explores the multiple threshold effects of UEL size, both directly on pollutants and in terms of its form's ability to reduce pollution, offering a deeper analysis than simply examining the linear effect of various metrics. (3) Based on empirical results, this study proposes differentiated UEL planning strategies for different units and the evolutionary UEL planning strategy for the same unit as it develops.

2. Materials and methods

2.1. Study area

The YREB (Fig. 1) stretches across China's eastern, central, and western regions, encompassing approximately 21% of China's land area. It includes eleven provinces linked by the Yangtze River: Sichuan, Chongqing, Guizhou, and Yunnan in the upper reaches; Hubei, Hunan, and Jiangxi in the middle reaches; and Shanghai, Jiangsu, Zhejiang, and Anhui in the lower reaches.

The YREB is chosen as the study area for the following reasons. Firstly, the YREB is a crucial region for China's economic and social development, contributing to over 40% of the nation's population and GDP. However, its rapid development has damaged the environment, with PM$_{2.5}$-O$_3$ composite pollution becoming a prominent atmospheric concern since 2015 (Wang et al., 2024a). Secondly, significant variation exists in urban development and land-use patterns across the YREB. Downstream cities are marked by rapid economic growth and intense urbanization, leading to larger urban areas and higher proportions of built-up land. In contrast, cities in the middle and upper reaches have smaller urban spaces, but they feature more ecological land within urban spaces and enjoy greater regional forest coverage (Wang et al., 2023b). Lastly, the region falls within the subtropical monsoon humid climate zone and the subtropical humid climate zone, promising similar meteorological conditions and vegetation types (Chen et al., 2023). This consistency helps minimize the influence of variations in local natural environments and urban ecological vegetation, enabling a more accurate analysis of the correlation between UEL and pollutant concentrations.

Besides, given that the county is the lowest-level administrative unit requiring formal master planning in China's current spatial planning system, 1068 counties in the YREB are chosen as the research units. Due to limitations in data availability, all data used in this study are from the year 2020.
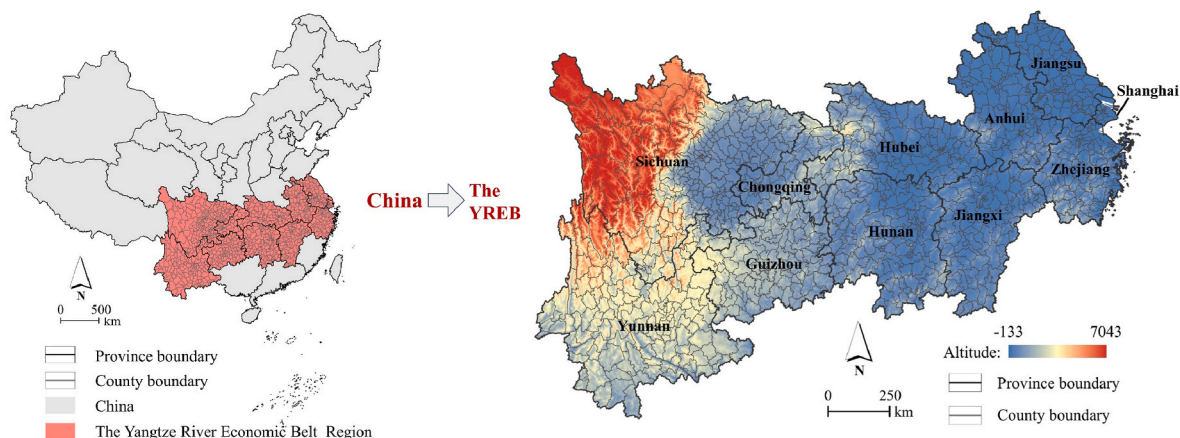

Fig. 1. Location of the YREB and research units in it.

2.2. Variables and data

This study employs the econometric model to examine the correlation between UEL and pollutant concentrations, as well as the potential threshold effect of UEL size on the UEL form's ability to reduce pollution. Therefore, $PM_{2.5}$ and O_3 concentrations are defined as the dependent variables in two separate models, with UEL size and form metrics serving as the core explanatory variables. UEL size is further incorporated as a threshold variable in the model fitting processes, quantified by the percent cover of UEL in the urban space. According to the studies on influencing factors of air pollution (detailed information is described in Text S1 and Fig. S1), regional land-use factors, socio-economic factors, and meteorological factors are selected as control variables, as shown in Table 1.

$PM_{2.5}$ and O_3 concentration data (1 km*1 km) are derived from ChinaHighAirPollutants (CHAP) datasets developed by Wei et al. (2021, 2022). The datasets are obtained using artificial intelligence and big data products (including ground-based observations, atmospheric reanalysis, and emission inventory production), with Ten-fold cross-validation R^2 for $PM_{2.5}$ and O_3 reaching 0.92 and 0.89, respectively. Land-use data (30m*30m) is derived from the annual China Land Cover Dataset (CLCD) developed by Yang and Huang (2023). Based on the Google Earth Engine platform, the dataset is produced by methods (including random forests, spatiotemporal filtering, and logical post-processing) on Landsat satellite imageries, with an overall classification accuracy of 79.31%. Night light data (1 km*1 km) is derived from NPP/VIIRSnight light data on the Earth Observation Group platform (https://eogdata.mines.edu/). Permanent population data (1 km*1 km) is derived from the Landscan population dataset (https://landscan.ornl.gov/). Temperature and precipitation data (1 km*1 km) are obtained from the Third Pole Environment Data Center Platform (TPDC, https://data.tpdc.ac.cn/). County data is from the Resource and Environment Data Cloud Platform (https://www.resdc.cn/).

2.3. Methods

2.3.1. UEL identification and landscape metrics

Firstly, urban space needs to be delineated from the broader regional territory, and ecological land within urban space should be identified based on existing land types. The first step involved extracting the regional territorial space (Fig. 3a) using the urban boundary (Fig. 3b), which was manually adjusted and visually inspected based on the 2018

Table 1
Variables and detailed indicators.

Variable type	Variable	Indicator	Acronym
Dependent variables	Pollutant concentrations	$PM_{2.5}$ concentration in the urban space; O_3 concentration in the urban space	$PM_{2.5}$; O_3
Core explanatory variables	UEL size (Threshold variable)	Percentage cover of UEL in the urban space	PEL
	UEL form	Listed in Table 2.	
Control variables	Regional land-use factors	Percentage cover of forest in the county; Percentage cover of water in the county	PFO; PWA
	Socio-economic factors	Nighttime light intensity in the urban space; Population density in the urban space	NTL; POP
	Meteorological factors	Precipitation in the urban space; Temperature in the urban space	PRE; TEM

Table 2
UEL form metrics computed in the study.

Metric (Acronym)	Formula and description	Significance
Area weighted mean shape index (AWMSI)	$AWMSI = \sum_{i=1}^{n} \left(0.25\, P_i \sqrt{S_i} \,/S\right)$ P_i and S_i respectively represents perimeter and area of UEL patch i; S represents total area of urban space.	Reflecting the regularity of patch shape; The larger value means greater complexity.
Patch density (PD)	$PD = n/S$ n represents the number of UEL patches; S represents total area of urban space.	Reflecting spatial fragmentation in unit of '1/hm²'; The larger value means greater fragmentation.
Splitting index (SPLIT)	$SPLIT = S^2 / \sum_{i=1}^{n} \ln\left(S_i^2\right)$ S_i represents area of UEL patch i; S represents total area of urban space.	Reflecting spatial separation; The larger value means greater separation.
Aggregation index (AI)	$AI = c_i /max \to c_i$ c_i represents number of similar adjacent UEL patches	Reflecting spatial aggregation in unit of '%'; The larger value means greater aggregation.
Shannon's diversity index (SHDI)	$SHDI = -\sum_{j=1}^{m=4} \left(p_j * \ln p_j\right)$ p_j represents percentage cover of UEL type j in urban ecological land, including forest, shrub, grassland, water, and wetland.	Reflecting functional richness of UEL; The larger value means greater richness.

Global Urban Boundary Dataset by Li et al. (2020) and 2020 satellite imagery. In the second step, green and blue spaces, which are interwoven and densely distributed within urban areas, collectively form UEL and provide ecological services (Feng et al., 2021; Wang et al., 2023c). Therefore, forest, shrub, grassland, water, and wetland among nine land types (Fig. 3a) are integrated and identified as UEL. All these steps are implemented in ArcGIS 10.6.

Then, landscape metrics from landscape ecology are used to quantify UEL forms. According to relevant studies (Fan and Myint, 2014; Ran et al., 2023; Shen et al., 2023), metrics are selected based on three principles: effectively reflecting the shape, distribution, and structure of the land; being easy to monitor and manage in practice; and applying to all units. The five selected metrics and their detailed information are provided in Table 2. All indicators are calculated using Fragstats 4.2.

2.3.2. Cross-sectional threshold regression model

Threshold regression involves setting a variable as the threshold variable and dividing the model into multiple segments based on its value, with each segment being regressed separately (Wang et al., 2022b). An effective threshold value can divide the data into two distinct sample groups, thereby allowing for comparing the model's performance at different threshold value intervals and gaining a more fine-grained understanding of correlations between variables (Tang and Wong, 2021). Since Tong (1983) introduced the threshold regression model, it has been widely used in testing nonlinear time series models in socio-economic fields. However, its application in the environmental domains has been relatively limited (Ouyang et al., 2019). Hansen (2000) extended the threshold regression model, making it applicable to cross-sectional data (Chen and Lee, 2005; Zheng et al., 2023). Based on data from 2020, this study employs a cross-sectional threshold regression model to analyze the threshold effect of PEL on correlations between pollutant concentrations and independent variables. The formulas are as follows:

$$Y_i = \mu_i + \theta_1 X_i \bullet I(q_i \leq \gamma_1) + \ldots + \theta_k X_i \bullet I(\gamma_{k-1} < q_i \leq \gamma_k) + \ldots$$

$$+ \theta_{n+1} X_i \bullet I(\gamma_n < q_i) + \varepsilon_i \tag{1}$$

$$I(con) = \begin{cases} 0, con = False \\ 1, con = True \end{cases} \quad (2)$$

In Eq. (1), Y_i and X_i represent dependent variable and series of independent variables of unit i, respectively; μ_i is the intercept parameter; ε_i is the error term. q_i is the threshold variable; γ_k represents the k-th threshold value; θ_k represents the series of coefficients which correspond to independent variables one by one, when q_i is in the k-th threshold interval. $I(con)$ is the indicator function (as detailed in Eq. (2)): It equals 0 when *con* is false, while equals 1 when *con* is true.

Successively taking all sample values as candidate thresholds and estimating corresponding θ_k using least squares estimation, the threshold value is identified when the sum of squared residuals of the model is minimized (Wang et al., 2021). Then to test threshold existence, this study first uses the bootstrap to calculate the p_value to determine the significance of the threshold effect. Subsequently, the 95% confidence interval of the threshold estimate and the likelihood ratio statistic are used to examine the closeness between the threshold estimate and the true value (Hansen, 1999). More detailed information can be found in the study by Chen and Lee (2005). Furthermore, the model was operated in Stata17.0.

2.3.3. Extended quadrant analysis

Quadrant analysis typically uses a four-quadrant model to classify samples into different types based on a binary classification of the sample's two indicators (Zhang et al., 2024), as shown in Fig. 2a. It has been effectively used in urban development and environmental research to classify research units (Hua et al., 2023; Wang et al., 2023a; Yu et al., 2024).

This study aims to provide tailored UEL planning strategies for different counties. Specifically, each county should optimize UEL forms based on UEL sizes to reduce $PM_{2.5}$ and O_3. That is, the primary pollutant and UEL size (quantized by PEL) are the two key attributes that determine the county type. However, with the possibility of multiple threshold values, PEL may be segmented into more than two categories, resulting in the formation of more than four quadrants when using the traditional four-quadrant model.

To address this issue, this study proposes an extended quadrant analysis, with the model shown in Fig. 2b. In the model, the Y-axis represents the PEL, divided into different intervals by threshold values. The series of X-axes are divided into two types with inverse directions, respectively representing two primary pollutants: $PM_{2.5}$ and O_3. Each

intersection of an X-axis and the Y-axis corresponds to a threshold value of PEL. To identify its quadrant within the model, each unit selects the Y-axis interval directly with its PEL and selects the X-axis interval by its primary pollutants (inferred as Eq. (3)). Consequently, all units are divided into several specific types, facilitating the formulation of differentiated planning strategies. Specifically, this study categorizes the counties in Excel and then visualizes the results in ArcGIS 10.6.

$$Pollu_i = \begin{cases} 'PM'_{2.5}, PM_{2.5i} \geq 10 \, and \, O_{3i} \geq 100 \, and \, Rank(PM_{2.5i}) < Rank(O_{3i}) \\ 'O'_3, PM_{2.5i} \geq 10 \, and \, O_{3i} \geq 100 \, and \, Rank(PM_{2.5i}) \geq Rank(O_{3i}) \\ 'PM'_{2.5}, PM_{2.5i} \geq 10 \, and \, O_{3i} \langle 100 \\ 'O'_3, PM_{2.5i} < 10 \, and \, O_{3i} \geq 100 \\ 'PM'_{2.5}, PM_{2.5i} < 10 \, and \, O_{3i} \langle 100 \, and \, Rank(PM_{2.5i}) < Rank(O_{3i}) \\ 'O'_3, \, PM_{2.5i} < 10 \, and \, O_{3i} \langle 100 \, and \, Rank(PM_{2.5i}) \geq Rank(O_{3i}) \end{cases}$$

$$(3)$$

In Eq. (3), $Pollu_i$ represents the primary pollutant of unit i; $PM_{2.5\,i}$ and $O_{3\,i}$ represent $PM_{2.5}$ and O_3 concentration of unit i, respectively; $Rank(Pollu)$ represents the descending ranking of pollutant concentration of unit i among all samples; 10 and 100 are the safety value of $PM_{2.5}$ and O_3 concentrations, respectively, set by the World Health Organization.

3. Results

3.1. Spatial distribution of UEL size and form

Three great plains dominated by cropland, water, and impervious surface can be identified in YREB (Fig. 3a): the Chengdu-Chongqing urban agglomeration in the upper reaches, the Wuhan urban agglomeration in the middle reaches, and the Jiangsu-Anhui region in the lower reaches. Western Sichuan is a grassland aggregation zone in the upstream area. The remaining regions of the YREB have higher forest coverage. Meanwhile, urban spaces (Fig. 3b) form several high-density agglomeration areas. Specifically, counties within the three aforementioned great plains have relatively larger urban boundaries and denser urban spaces. Other regions have also formed clusters of urban spaces centered around economically developed counties within each province.

Fig. 3c–h illustrate UEL size and form metrics for each county. The spatial distributions of PEL, AWMSI, and PD are similar and consistent with the distribution of regional ecological land coverage. Specifically,
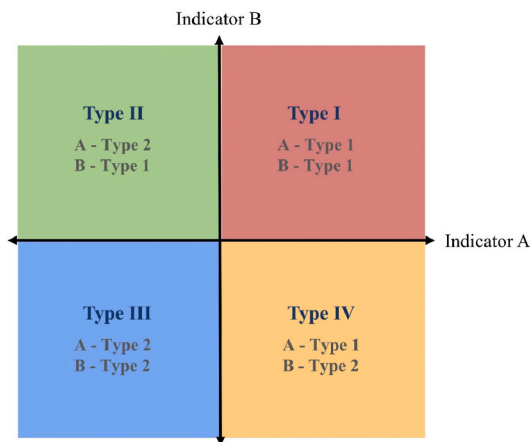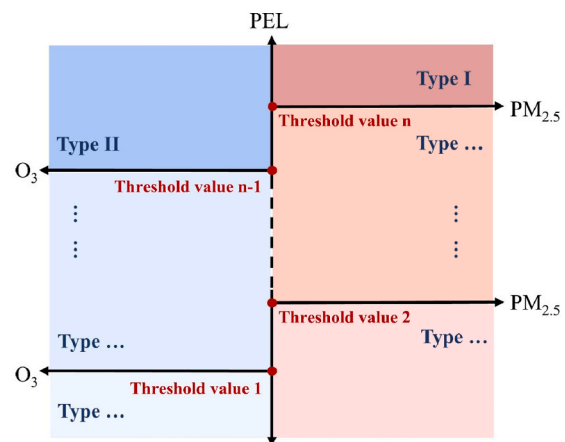

Fig. 2. Four-quadrant model and extended quadrant model in this study.
Note: the colors in Fig. 2a ~ Fig. 2b are for quadrant distinction and aesthetics, without scientific meaning.
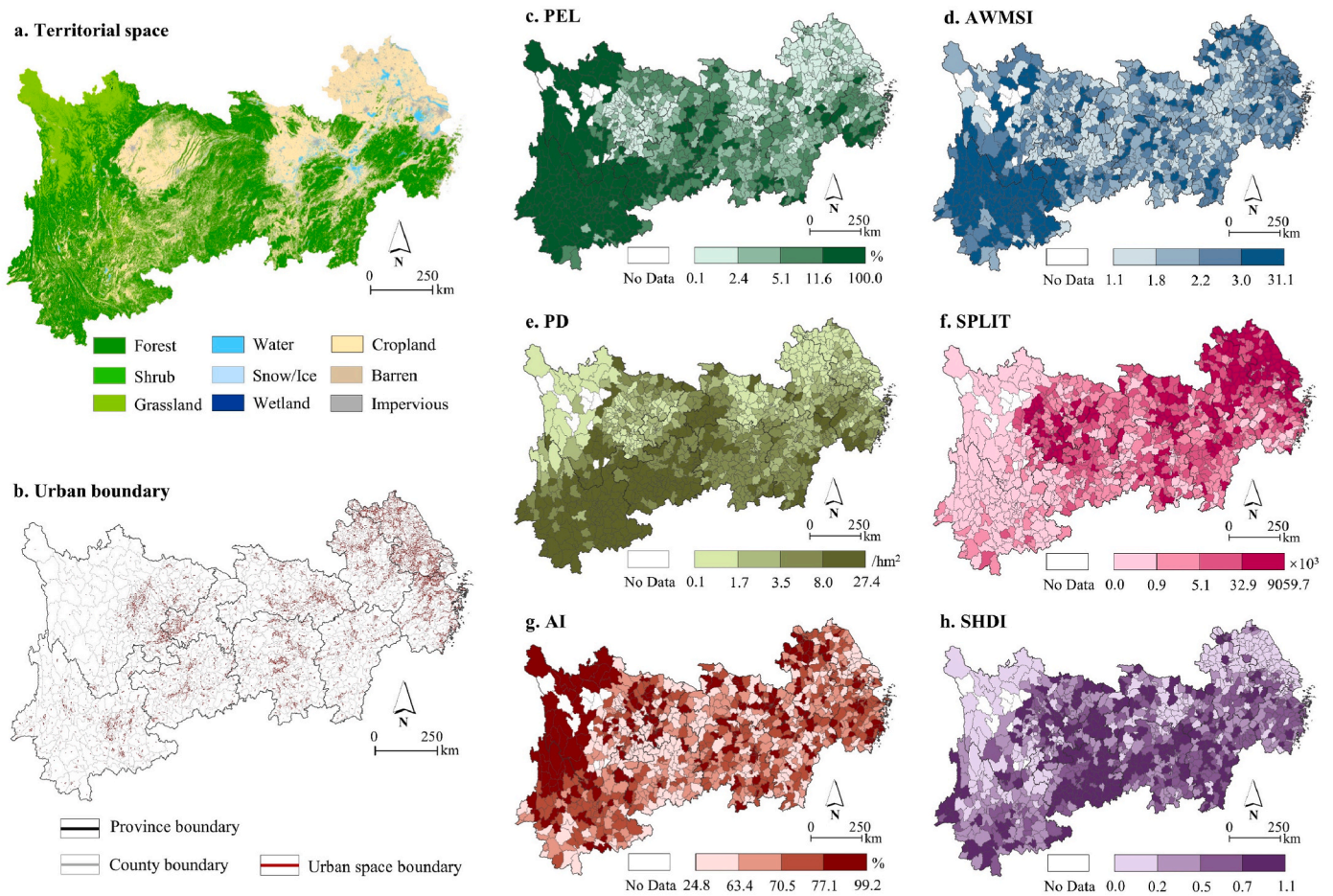
Fig. 3. UEL size and form metrics of counties.
Note: UEL form metrics in Fig. 3c ~ Fig. 3h are all classified by quantile grading method.

in upstream Yunnan, Chongqing-Hubei border area in the middle reaches, and southern Zhejiang in the downstream, ecological lands occupy a large proportion of the county area, forcing urban spaces to be developed in the limited available areas. As a result, ecological lands take larger proportions of urban spaces within those counties, exhibiting greater shape complexity and spatial fragmentation. SPLITs of UELs in counties within three great plains are relatively larger, corresponding to their smaller UEL sizes and the scattered distribution of UELs among croplands and impervious surfaces. AI of UEL varies significantly across counties, with no distinct spatial clustering observed. Additionally, except for the relatively homogeneous ecological land types in the grasslands of western Sichuan, the forests of Yunnan, and the croplands of northern Jiangsu, SHDIs of UELs are generally higher in counties from other regions.

3.2. Spatial distribution of PM_{2.5} and O_3 concentrations in urban spaces

Fig. 4a and b presents $PM_{2.5}$ and O_3 concentrations in the urban space of each county. $PM_{2.5}$ concentrations in urban spaces form significant high-value cores in three great plains, with values decreasing in a ring-like pattern outward. This is related to the relatively intense socio-economic development in great plains, leading to more particulate

matter emissions and relatively less ecological land within the urban spaces. O_3 concentrations in urban areas form significant high-value zones in the middle and lower reaches, while low-value zones appear in Chongqing and Guizhou in the upper reaches. Meanwhile, O_3 concentrations in the urban areas of Sichuan and Yunnan, also in the upper reaches, show considerable variation between counties, generally remaining at moderate levels without forming significant spatial clustering.

Furthermore, both numerical and spatial correlations between $PM_{2.5}$ and O_3 concentrations have been calculated to assess the feasibility of coordinated control of composite pollution (details of methods are described in Text S2), as shown in Fig. 4c and d. The results show an overall positive correlation (0.580) between pollutant concentrations in urban spaces of all counties, which passes the significance test. This correlation is stronger in most units where $PM_{2.5}$ concentrations exceed 20 μg/m^3, suggesting that controlling one pollutant could help reduce the other within the same county. Regarding spatial correlation, severe and mild pollution clusterings are observed in the northeastern YREB and the Guizhou-western Yunnan area and its surroundings, respectively. In these regions, controlling one pollutant in a county can affect the other pollutant concentrations in neighboring counties.
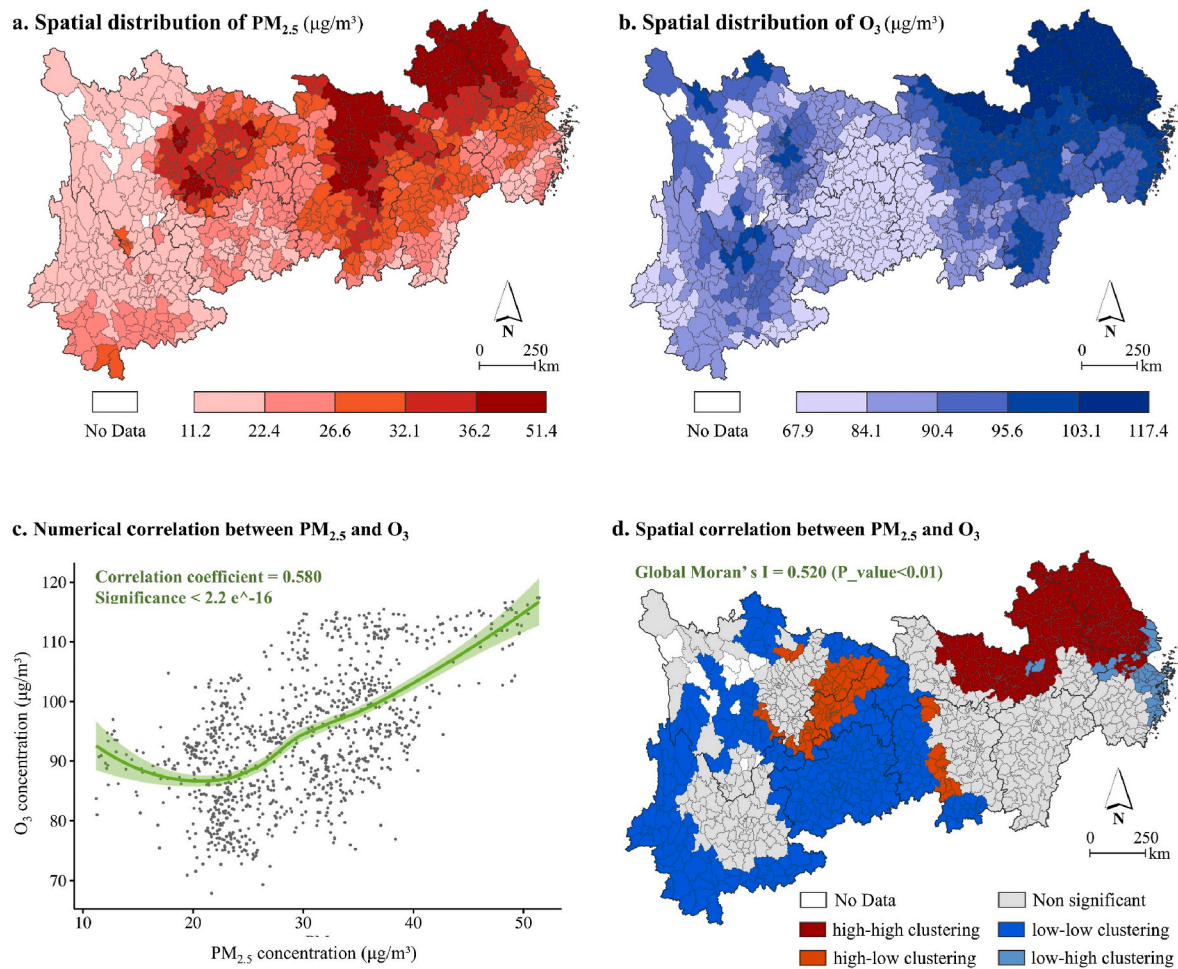
a. Spatial distribution of PM$_{2.5}$ (µg/m³)

b. Spatial distribution of O$_3$ (µg/m³)

c. Numerical correlation between PM$_{2.5}$ and O$_3$

d. Spatial correlation between PM$_{2.5}$ and O$_3$

Fig. 4. Spatial distribution of PM$_{2.5}$ and O$_3$ concentrations and their numerical and spatial correlations.
Note: (1) numerical correlation between PM$_{2.5}$ and O$_3$ (Fig. 4c) is evaluated by Pearson correlation coefficient, with locally weighted scatterplot smoothing being mapped; (2) spatial correlation between PM$_{2.5}$ and O$_3$ (Fig. 4d) is assessed by bivariate spatial autocorrelation analysis, with global Moran's I index being labeled and results of local Moran's I being mapped.

3.3. Threshold effects of PEL

3.3.1. Results of threshold existence tests

The variance inflation factors (VIF) of the independent variables are first calculated for collinearity analysis. As Table S1 presented, all variables passed the test, with VIF values less than 5. Then, threshold values and threshold effects of PEL (quantizing UEL size) are calculated and tested, with PM$_{2.5}$ and O$_3$ concentrations as the dependent variables, respectively.

Table 3 presents the estimated threshold values, the significance tests for threshold effects, and the number of samples within each interval defined by threshold values. For PM$_{2.5}$, the significance tests confirm the presence of single, double, triple, and quadruple threshold effects of PEL. However, when applying the quadruple threshold, only 26 samples

fall into the last interval (PEL >82.230%), which is insufficient for producing a valid regression result. Therefore, the fourth threshold should be excluded. For O$_3$, the significance tests confirm the presence of double threshold effects. However, when using the double threshold, the number of samples in the last interval (PEL >91.069%) is only 18, which is insufficient for a valid regression result. Similarly, the second threshold should be excluded.

Furthermore, the proximity of the estimated threshold value to the true value is assessed using the 95% confidence interval test (as presented in Table 3) and the likelihood ratio statistic results (as illustrated in Fig. S2). The results indicate that the 95% confidence intervals for the selected threshold values are all within a narrow range, successfully passing the test. As a result, PEL demonstrates significant triple

Table 3
Test results of threshold existences of PEL.

Pollutant	Threshold order	Threshold value (%)	p_value	95% confidence interval	Number of samples in different stages
PM$_{2.5}$	The first threshold	4.302	0.000	[4.260, 4.496]	(468, 590)
	The second threshold	8.055	0.000	[7.622, 14.275]	(468, 220, 370)
	The third threshold	23.742	0.000	[21.688, 30.850]	(468, 220, 234,136)
	The fourth threshold	82.230	0.037	[82.230, 83.123]	(468, 220, 234,110, 26)
O$_3$	The first threshold	3.275	0.000	[3.275, 3.275]	(370, 688)
	The second threshold	91.069	0.000	[91.144,91.910]	(370, 670, 18)

Note: (1) two-thousand bootstrap replications are employed for each bootstrap test to calculate the p_value; (2) this study takes p_value <0.1 as passing the test; (3) due to ten counties lacking urban boundary data, the number of samples in the study is 1058.

threshold effects in the regression model for PM$_{2.5}$ concentration, with threshold values of 4.302%, 8.055%, and 23.742%. Meanwhile, PEL exhibits a single threshold effect in the regression model for O$_3$ concentration, with a threshold value of 3.275%.

3.3.2. Results of cross-sectional threshold regression model

Table 4 presents the results of threshold regression models for pollutant concentrations, with independent variables including UEL form metrics. When PEL ≤4.302%, PEL, AWMSI, PD, and SPLIT are all significantly negatively correlated with PM$_{2.5}$ concentration. When 4.302% < PEL ≤8.055%, only SHDI shows a significant positive correlation with PM$_{2.5}$ concentration. When 8.055% < PEL ≤23.742%, PEL, and AWMSI are significantly negatively correlated with PM$_{2.5}$ concentration, while AI shows a significant positive correlation with PM$_{2.5}$ concentration. Additionally, when PEL ≤3.275%, AWMSI and SHDI show a significant positive and negative correlation with O$_3$ concentration, respectively. When PEL >3.275%, PEL and SHDI are significantly negatively correlated with O$_3$ concentration, while SPLIT shows a positive correlation with O$_3$ concentration.

Noticeably, as PEL enters larger value intervals, neither UEL size nor form metrics are consistently significantly correlated with pollutant concentrations. When a variable is significantly correlated with a pollutant concentration across different PEL intervals, the sign of the correlation coefficient generally remains consistent. For example, PEL, AWMSI, SPLIT, and SHDI show this pattern in relationship to PM$_{2.5}$ concentration. Additionally, the correlations of AWMSI, SPLIT, and SHDI with O$_3$ concentration exhibit the opposite trend compared to their

correlations with PM$_{2.5}$ concentration, although the PEL intervals in which their effects are significant do not perfectly align.

Furthermore, this study performs a robustness check by rerunning the regression after removing the control variables. The details of the test are provided in Text S3, Tables S2–S3, and Fig. S3. The results indicate that removing the control variables affects the numerical relationships between UEL (size and form) and pollutant concentrations. However, the threshold effects of UEL size remain highly consistent, as evidenced by the consistency in the number of thresholds and the proximity of the threshold values. Therefore, the threshold regression results are considered robust and valid.

3.4. Categorization and differentiated planning strategies of counties

Based on the extended quadrant model proposed in this study, the categorization of counties and their spatial distribution are illustrated in Fig. 5. Six types have been identified according to the county's primary pollutant and UEL size.

Counties categorized as type I to IV should prioritize reducing PM$_{2.5}$. Type IV counties are the most numerous and exhibit significant spatial clustering, including the Chengdu-Chongqing urban agglomeration in the upper reaches, the Wuhan urban agglomeration and northern Jiangxi in the middle reaches, and northern Anhui in the lower reaches. For these counties with relatively small PELs, the introduction of more dispersed and irregularly shaped UELs can effectively reduce particulate matter in urban spaces. Type I counties are relatively few, concentrated in western Sichuan and western Yunnan in the upper reaches. For these

Table 4
Results of threshold regression models for pollutant concentrations and independent variables.

PEL (%)	PM$_{2.5}$				O$_3$	
	[0.000, 4.302]	(4.302, 8.055]	(8.055, 23.742]	(23.742, 100.000)	[0.000, 3.275]	(3.275, 100.000)
R^2	0.609	0.479	0.566	0.744	0.620	0.329
PEL	−1.423*	0.102	−0.193*	−0.115***	−0.102	−0.121*
AWMSI	−1.649***	0.034	−1.119***	−0.040	1.150*	−0.034
PD	−2.148***	−0.219	−0.033	0.201*	−0.578	−0.124
SPLIT	−0.000*	−0.000	0.000	−0.003*	−0.000	0.000**
AI	0.025	0.009	0.308**	0.189	0.084	0.211
SHDI	−0.216	3.145*	−0.236	2.997*	−4.707**	−5.840***
PFO	−0.130	−0.138***	−0.064***	−0.063***	−0.112***	−0.061**
PWA	−0.134***	−0.020	0.046	0.137*	0.227***	0.328***
NTL	−0.357*	−0.100	−0.071	−0.001	−0.087	0.232***
POP	0.000	−0.000	0.000	0.000	0.000*	−0.000*
PRE	−0.084*	0.051*	0.013	0.033**	0.093***	−0.040*
TEM	−1.202**	−0.503*	0.091	0.306**	−5.088***	0.416*

Note: as for the significance test, * represents p_value <0.1; ** represents p_value <0.01; *** represents p_value < 0.001.
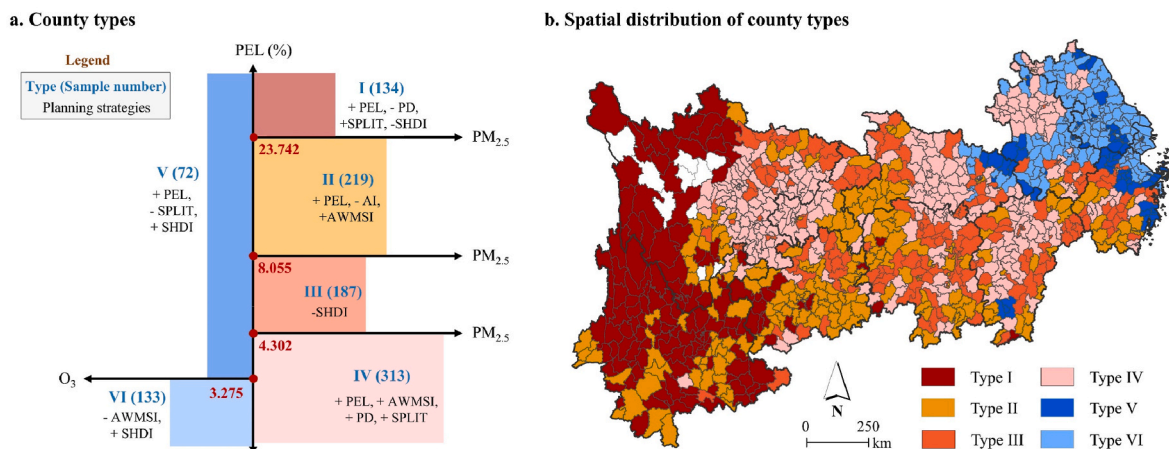

Fig. 5. Categorization of counties and their spatial distribution.

counties with relatively large PELs, consolidating smaller patches into larger units and strategically dispersing them next to non-ecological land could enhance their potential for PM$_{2.5}$ reduction. Type II counties are mainly concentrated in the southern mid-upper reaches and the Chongqing-Hubei border area, where moderately sized clusters of UEL have already developed. To further enhance PM$_{2.5}$ reduction, these counties should increase the size of UEL while reducing its aggregation and increasing its shape complexity to maximize the interaction area with particulate matter. Type III counties are dispersed across the mid-lower reaches. A key planning strategy for these counties to directly reduce particulate matter is to increase the uniformity of UEL types.

Counties categorized as type V and VI, primarily located in lower reaches such as Shanghai, Jiangsu, northern Zhejiang, and central Anhui, should prioritize the reduction of O$_3$. Type V counties are the fewest in number, forming several distinct point-like clustering: Taizhou, Shaoxing, and Huzhou in Zhejiang; Suzhou in Jiangsu; and Huanggang in Hubei. The planning strategy for these counties includes increasing the size and typological diversity of UEL while minimizing its fragmentation. Type VI counties are primarily clustered in Jiangsu and central Anhui. For these counties with small PEL, reducing the shape complexity of UEL while increasing its typological diversity can better reduce ozone concentrations in urban space.

4. Discussion

4.1. Potential mechanism of the matching between UF size and form

4.1.1. Explanation of the threshold effect of UEL size

To better understand the threshold effects of PEL, it is necessary to recognize the potential mechanisms by which UEL affects pollutant concentrations. On the one hand, UEL can directly reduce the generation of PM$_{2.5}$ and O$_3$ by replacing pollution sources in non-ecological land and through soil nitrogen fixation (Lu et al., 2020; Wu et al., 2021). On the other hand, UEL affects pollutant concentrations primarily through its land cover, including forests, shrubs, grasslands, and water bodies (Qian et al., 2024; Zhou et al., 2021). Moreover, existing research suggests that the specific form of land cover can alter its functional capacity, thereby influencing its correlation with pollutant concentrations (Yang et al., 2022). As a result, changes in land size have a stronger impact on the pollution reduction capabilities of the land cover than on its intrinsic ecological functions, which is crucial for understanding the size threshold effects.

Therefore, this study proposes that the scale effects of land cover and the diminishing marginal returns of its pollution reduction capabilities can potentially explain the threshold effects of UEL size. When the size of ecological land reaches a certain threshold, the vegetation or water bodies within it can form a cohesive unit that effectively influences atmospheric pollutants, thereby amplifying the impact of its form characteristics (Lin et al., 2020). Additionally, as UEL size continues to increase along with its land cover expanding, the marginal effect on pollutant concentration diminishes (Vaz Monteiro et al., 2016). Specifically, the area of non-ecological land decreases, the remaining pollutants that can be reduced become limited, and the pollution reduction capacity of the land cover approaches saturation, making it difficult to further unlock the potential of UEL by adjusting size and form (Chen and Wei, 2024; Hu et al., 2020b). Given that UF form influences the degree of UF's functioning, it can be further inferred that the pollution reduction capacity of UF will exhibit a specific tendency related to its form at different UF sizes.

4.1.2. Analysis of UEL form performance across size intervals

Regarding the issue of UEL size intervals, the threshold effects of ecological land size are initially explored in urban cooling studies. Peng et al. (2016) found that at the 6*6m grid scale, the optimal ecological land coverage for effective cooling exceeds 70%, which was later supported by Liu et al. (2018b). This study identifies the lower threshold

values of PEL influencing pollutant concentrations: 4.302%, 8.055%, and 23.742% for PM$_{2.5}$; and 3.275% for O$_3$. Given that the study focuses on urban spaces with numerous emission sources, it suggests that even small proportions and changes in ecological elements can have a significant impact when concentrated in urban spaces. This finding is consistent with that of Ren et al. (2023): at the territorial space scale, the optimal coverage for cooling effects is 20% for forests, 0.1% for shrubs, 42.5% for grasslands, and 15.4% for water bodies. Therefore, at the urban space scale, it is crucial to conduct detailed planning of UEL that incorporates various finer types (Liu et al., 2014).

Existing studies have examined the mechanism by which UEL affects PM$_{2.5}$ concentrations. Specifically, vegetation and water bodies serve as both absorbers and emitters of PM$_{2.5}$, with absorption typically overweighing emissions (Abhijith et al., 2017; Shen et al., 2023). When UEL forms a larger whole, it can indirectly affect PM$_{2.5}$ concentrations by adjusting the local microclimate (Santiago and Rivas, 2021). This study further provides a size and form perspective into the above mechanisms. Firstly, no threshold has been observed for UEL to exhibit a scale effect, although its diminishing marginal returns have already set in. This is reflected in the continuing decline of the correlation coefficients between PM$_{2.5}$ concentrations and UEL form metrics. Secondly, AWMSI plays a key role in reducing PM$_{2.5}$ when PEL is less than 4.302% or falls within 8.055%–23.742%, while a larger SPLIT reduces PM$_{2.5}$ when PEL is below 3.275% or exceeds 23.742%. Greater shape complexity and patch separation indicate more opportunities for interaction with non-ecological lands. This study suggests that such interactions enhance the removal of PM$_{2.5}$ from built-up areas, which aligns with the findings of Chen et al. (2017) and Wang et al. (2022a). However, Cai et al. (2020) found that aggregated green space facilitates PM$_{2.5}$ reduction. We propose that this discrepancy may arise from the fact that their study was conducted within a buffer zone, whereas ours was conducted on a regional scale. Thirdly, SHDI shows a positive correlation with PM$_{2.5}$ concentrations when PEL is within 4.302%~8.055% or exceeds 23.742%. Typological diversity is a common strategy in urban planning to enhance aesthetics and maximize land use benefits (Lam and Conway, 2018). However, the findings above offer new insights for relevant practices from the perspective of PM$_{2.5}$ reduction: uniformity in land types could also be useful.

Regarding the reduction of O$_3$, UEL can reduce ozone primarily through dry deposition but also generate ozone indirectly by releasing O$_3$ precursors, leading to an uncertain impact on O$_3$ concentrations (Qu et al., 2023; Taha et al., 2016). Based on the study results, we propose several insights into the potential mechanisms. Firstly, we suggest the existence of a threshold for the scale effect of UEL in reducing ozone, as evidenced by the significant correlation between PEL and O$_3$ concentrations once PEL exceeds 3.275%. This demonstrates the rationale for continuing nature-based planning practices, such as afforestation and ecological restoration (Wang et al., 2024b). Secondly, AWMSI is positively correlated with O$_3$ when PEL is below 3.275%, while a larger SPLIT increases O$_3$ when PEL exceeds 3.275%. This study suggests that increased interactions between UEL and built-up land will release ozone precursors into urban space, resulting in pollution scenarios similar to those observed by Han et al. (2024). Furthermore, it can be inferred that the contribution of ecological land to the release of ozone precursors may outweigh its role in the dry deposition of ozone, which meets the findings of Han et al. (2024). Thirdly, SHDI is negatively correlated with O$_3$ concentrations across both identified intervals. UEL in this study includes forest, shrub, grassland, water, and wetland, containing both vegetation and water bodies. Therefore, we propose that further research should explore the relationships between various UEL types and ozone concentrations.

4.2. Evolutionary planning strategy of UEL

There are several trade-offs in UEL planning. When setting planning objectives, it is necessary to consider ecological, economic, and cultural

benefits. However, emphasis should be placed on specific aspects depending on the stage of development and the region. This study focuses on addressing the PM$_{2.5}$–O$_3$ composite pollution currently affecting China. In terms of planning content, key trade-offs include prioritizing either an increase in quantity or the optimization of form; selecting between regular or irregular shapes, as well as aggregation or dispersion; and deciding whether to emphasize diversity or uniformity in types (Leitão and Ahern, 2002; Wang et al., 2001). To address these issues, different cities should implement differentiated UEL planning strategies tailored to their specific conditions (Fei et al., 2019). However, existing studies often categorize the entire sample based on external conditions, such as development level and geographical location (Chen et al., 2019; Liang and Gong, 2020), while neglecting the stage-specific characteristics of UEL development (Yao et al., 2021). The findings of this study provide a new approach: make planning strategies to optimize UEL form based on UEL size.

As illustrated in Fig. 6, the planning strategy of the UEL form should evolve as the UEL size increases. Specifically, assuming that forest, shrub, grassland, water, and wetland are distributed as patches within the region, each land type is represented by a distinct color. These patches have attributes, including area and shape complexity, and collectively exhibit characteristics such as aggregation and continuity, which can be directly interpreted from the figure. Based on the research results, four stages of UEL form optimization for PM$_{2.5}$ reduction and two stages for O$_3$ reduction are proposed, which can be further specified based on the characteristics of each county.

Four stages of UEL planning to reduce PM$_{2.5}$ are proposed. (1) The scatter-growth mode is when the UEL size is relatively small, and PM$_{2.5}$ reduction is achieved by increasing irregularly shaped UEL in various locations. Considering that the UEL required at this stage consists of relatively small land patches, private gardens, roadside green spaces, and other similar areas (Silveira et al., 2024) can serve as the effective carrier applicable to various counties. (2) The individualized mode emerges when UEL size enters the next interval, and maintaining the uniformity of UEL types can help reduce particulate matter. Since the impact of UEL form metrics is limited at this stage, form optimization can be tailored to counties' individualized characteristics. For example, in the Jiangnan water towns with rich water resources, an ecological land network can be constructed by connecting rivers (Zhou et al., 2024). In counties within mountainous areas, multi-core development

can be centered around the main mountain ranges (Yu et al., 2018). (3) The localized assembly mode occurs when UEL size surpasses the second threshold, marking the stage where previously scattered patches are connected nearby to form a system. Counties with better economic development can establish artificial ecological corridors to connect patches, while counties with stronger ecological endowments can achieve this by identifying potential plots that can be converted into ecological land. (4) In multicenter mode, UEL forms significant concentration centers in different areas, while these centers maintain separation from each other to alleviate diminishing marginal returns.

Two stages of UEL planning to reduce O$_3$ are also proposed. (1) In the trimming mode, when the UEL size is relatively small, shaping it into more regular shapes helps reduce the influx of ozone precursors into built-up areas. At this stage, counties can further divide UEL into areas within the urban core and those adjacent to the urban-rural fringe. The optimization of UEL at the urban-rural fringe needs to be paid more attention and potentially integrated with the demarcation of urban development boundaries (Cui et al., 2020; Xie et al., 2024). (2) The clustering mode occurs when UEL size suppresses threshold values, generating scale effects of pollution reduction. During this stage, UEL should be aggregated to further form the regional UEL network (Teng et al., 2016) and the diversity of UEL types should be maximized. Overall, PM$_{2.5}$ reduction requires a dispersed UEL form to increase its interaction surface with non-ecological lands and enhance the uniformity of UEL types. In contrast, the O$_3$ reduction necessitates the aggregation of UEL and an increase in the diversity of UEL types. As the primary pollutant changes during county development, UEL planning strategies should be promptly and accurately adjusted.

4.3. Limitations and prospects

This study has several limitations. Firstly, due to limited data availability, only two-dimensional landscape metrics were used to quantify UEL form. Future research could incorporate three-dimensional morphological metrics to supplement these analyses. Secondly, the study identifies each county's primary pollutant by ranking its two pollutant concentrations relative to those of all counties. While this approach aligns with governmental performance comparison needs, examining more units may make the results less stable. Future studies could develop specific indicators for more consistent assessments.
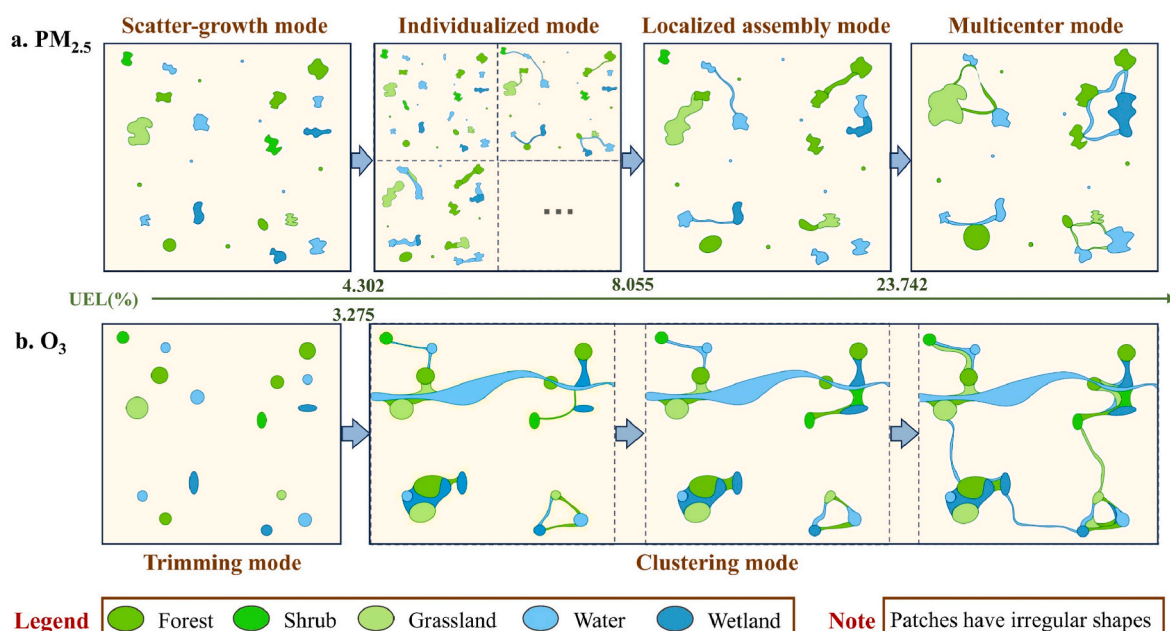

Fig. 6. The Evolutionary planning strategy of UEL to reduce PM$_{2.5}$ and O$_3$.

Thirdly, this study utilizes static cross-sectional data, lacking an analysis of temporal changes. Future research could explore dynamic relationships between UEL and pollutant concentrations using more fined data and dynamic models.

5. Conclusions

This study focuses on governing $PM_{2.5}$-O_3 composite pollution through strategic planning of UEL, with particular emphasis on optimizing UEL form based on its size thresholds. Forest, shrub, grassland, water, and wetland in the urban space are integrated into UEL as a whole. The cross-sectional threshold regression model is used to explore the threshold effects of UEL size, examining how the correlations between UEL form metrics and pollutant concentrations vary across UEL size intervals. Quadrant analysis is extended to categorize counties based on their primary pollutants and UEL sizes. The main conclusions can be summarized as follows: (1) UEL size exhibits a triple threshold effect on the regression of $PM_{2.5}$ at 4.302%, 8.055%, and 23.742%, and a single-threshold effect on the regression of O_3 at 3.275%. Each UEL form metric shows different significances and similar coefficient signs across UEL size intervals within the regression for the same pollutant. (2) Counties are categorized into six types, each associated with specific optimization strategies for the UEL form. Counties of the same type exhibit a certain degree of spatial clustering. (3) Overall, dispersed and irregularly shaped UEL is more effective in reducing $PM_{2.5}$, while these patches could have greater potential if aggregated into several centers once the UEL size exceeds 23.742%. Meanwhile, O_3 reduction consistently benefits more from aggregated and diverse UEL, with the potential size threshold for the scale effects occurring at 3.275%. (4) The evolutionary UEL planning strategy is proposed to match the expansion of UEL at the county level. Specifically, four and two stages are proposed to reduce $PM_{2.5}$ and O_3, respectively.

CRediT authorship contribution statement

Xin Chen: Writing – review & editing, Writing – original draft, Visualization, Software, Methodology, Formal analysis, Data curation, Conceptualization. **Fang Wei:** Writing – review & editing, Supervision.

Declaration of generative AI and AI-assisted technologies in the writing process

During the preparation of this work, the authors used ChatGPT to assist with grammar and spelling. After using this tool, the authors have carefully reviewed and edited the content as needed and assumed full responsibility for the publication's content.

Declaration of competing interest

The authors declare that they have no known competing financial interests or personal relationships that could have appeared to influence the work reported in this paper.

Appendix A. Supplementary data

Supplementary data to this article can be found online at https://doi.org/10.1016/j.apr.2025.102466.

References

Abhijith, K.V., Kumar, P., Gallagher, J., McNabola, A., Baldauf, R., Pilla, F., Broderick, B., Di Sabatino, S., Pulvirenti, B., 2017. Air pollution abatement performances of green infrastructure in open road and built-up street canyon environments – a review. Atmos. Environ. 162, 71–86. https://doi.org/10.1016/j.atmosenv.2017.05.014.

Bi, S., Chen, M., Dai, F., 2022. The impact of urban green space morphology on PM2.5 pollution in Wuhan, China: a novel multiscale spatiotemporal analytical framework. Build. Environ. 221, 109340. https://doi.org/10.1016/j.buildenv.2022.109340.

Cai, L., Zhuang, M., Ren, Y., 2022. Spatiotemporal characteristics of NO2, PM2.5 and O3 in a coastal region of southeastern China and their removal by green spaces. Int. J. Environ. Health Res. 32, 1–17. https://doi.org/10.1080/09603123.2020.1720620.

Cai, L., Zhuang, M., Ren, Y., 2020. A landscape scale study in Southeast China investigating the effects of varied green space types on atmospheric PM2.5 in mid-winter. Urban For. Urban Green. 49, 126607. https://doi.org/10.1016/j.ufug.2020.126607.

Chen, A., Yao, X.A., Sun, R., Chen, L., 2014. Effect of urban green patterns on surface urban cool islands and its seasonal variations. Urban For. Urban Green. 13, 646–654. https://doi.org/10.1016/j.ufug.2014.07.006.

Chen, L., Liu, C., Zhang, L., Zou, R., Zhang, Z., 2017. Variation in tree species ability to capture and retain airborne fine particulate matter (PM2.5). Sci. Rep. 7, 3206. https://doi.org/10.1038/s41598-017-03360-1.

Chen, M., Dai, F., Yang, B., Zhu, S., 2019. Effects of urban green space morphological pattern on variation of PM2.5 concentration in the neighborhoods of five Chinese megacities. Build. Environ. 158, 1–15. https://doi.org/10.1016/j.buildenv.2019.04.058.

Chen, M., Jia, W., Du, C., Shi, M., Henebry, G.M., Wang, K., 2023. Carbon saving potential of urban parks due to heat mitigation in Yangtze River Economic Belt. J. Clean. Prod. 385, 135713. https://doi.org/10.1016/j.jclepro.2022.135713.

Chen, S.-T., Lee, C.-C., 2005. Government size and economic growth in Taiwan: a threshold regression approach. J. Policy Model. 27, 1051–1066. https://doi.org/10.1016/j.jpolmod.2005.06.006.

Chen, X., Wei, F., 2024. Impact of territorial spatial landscape pattern on PM2.5 and O3 concentrations in the Yangtze River delta urban agglomeration: exploration and planning strategies. J. Clean. Prod. 452, 142172. https://doi.org/10.1016/j.jclepro.2024.142172.

Cui, L., Wang, J., Sun, L., Lv, C., 2020. Construction and optimization of green space ecological networks in urban fringe areas: a case study with the urban fringe area of Tongzhou district in Beijing. J. Clean. Prod. 276, 124266. https://doi.org/10.1016/j.jclepro.2020.124266.

Fan, C., Myint, S., 2014. A comparison of spatial autocorrelation indices and landscape metrics in measuring urban landscape fragmentation. Landsc. Urban Plan. 121, 117–128. https://doi.org/10.1016/j.landurbplan.2013.10.002.

Fan, H., Yu, Z., Yang, G., Liu, Tsz Yiu, Liu, Tsz Ying, Hung, C.H., Vejre, H., 2019. How to cool hot-humid (Asian) cities with urban trees? An optimal landscape size perspective. Agric. For. Meteorol. 265, 338–348. https://doi.org/10.1016/j.agrformet.2018.11.027.

Fan, Z., Zhan, Q., Liu, H., Wu, Y., Xia, Y., 2022. Investigating the interactive and heterogeneous effects of green and blue space on urban PM2.5 concentration, a case study of Wuhan. J. Clean. Prod. 378, 134389. https://doi.org/10.1016/j.jclepro.2022.134389.

Fei, J., Xia, J., Hu, J., Shu, X., Wu, X., Li, J., 2019. Research progress of ecological space and ecological land in China. Chin. J. Eco-Agric. 27, 1626–1636.

Feng, R., Wang, F., Wang, K., Wang, H., Li, L., 2021. Urban ecological land and natural-anthropogenic environment interactively drive surface urban heat island: an urban agglomeration-level study in China. Environ. Int. 157, 106857. https://doi.org/10.1016/j.envint.2021.106857.

Gómez-Baggethun, E., Barton, D.N., 2013. Classifying and valuing ecosystem services for urban planning. Ecol. Econ. 86, 235–245. https://doi.org/10.1016/j.ecolecon.2012.08.019.

Guan, Y., Xiao, Y., Wang, F., Qiu, X., Zhang, N., 2021. Health impacts attributable to ambient PM2.5 and ozone pollution in major Chinese cities at seasonal-level. J. Clean. Prod. 311, 127510. https://doi.org/10.1016/j.jclepro.2021.127510.

Han, L., Zhang, R., Wang, J., Cao, S.-J., 2024. Spatial synergistic effect of urban green space ecosystem on air pollution and heat island effect. Urban Clim. 55, 101940. https://doi.org/10.1016/j.uclim.2024.101940.

Han, L., Zhao, J., Gao, Y., Gu, Z., 2022. Prediction and evaluation of spatial distributions of ozone and urban heat island using a machine learning modified land use regression method. Sustain. Cities Soc. 78, 103643. https://doi.org/10.1016/j.scs.2021.103643.

Hansen, B.E., 2000. Sample splitting and threshold estimation. Econometrica 68, 575–603. https://doi.org/10.1111/1468-0262.00124.

Hansen, B.E., 1999. Threshold effects in non-dynamic panels: estimation, testing, and inference. J. Econom. 93, 345–368. https://doi.org/10.1016/S0304-4076(99)00025-1.

Hu, L., Sun, Y., Collins, G., Fu, P., 2020a. Improved estimates of monthly land surface temperature from MODIS using a diurnal temperature cycle (DTC) model. ISPRS J. Photogramm. Remote Sens. 168, 131–140. https://doi.org/10.1016/j.isprsjprs.2020.08.007.

Hu, T., Li, X., Gong, P., Yu, W., Huang, X., 2020b. Evaluating the effect of plain afforestation project and future spatial suitability in Beijing. Sci. China Earth Sci. 63, 1587–1598. https://doi.org/10.1007/s11430-019-9636-0.

Hua, Z., Chen, Y., Zeng, Z., Wu, Z., 2023. Spatiotemporal coupling analysis between human footprint and ecosystem service value in the highly urbanized Pearl River Delta urban Agglomeration, China. Ecol. Indic. 148, 110033. https://doi.org/10.1016/j.ecolind.2023.110033.

Hunter, R.F., Cleland, C., Cleary, A., Droomers, M., Wheeler, B.W., Sinnett, D., Nieuwenhuijsen, M.J., Braubach i, M., 2019. Environmental, health, wellbeing, social and equity effects of urban green space interventions: a meta-narrative evidence synthesis. Environ. Int. 130, 104923. https://doi.org/10.1016/j.envint.2019.104923.

Knippertz, P., Evans, M.J., Field, P.R., Fink, A.H., Liousse, C., Marsham, J.H., 2015. The possible role of local air pollution in climate change in West Africa. Nat. Clim. Change 5, 815–822. https://doi.org/10.1038/nclimate2727.

Lam, S.T., Conway, T.M., 2018. Ecosystem services in urban land use planning policies: a case study of Ontario municipalities. Land Use Policy 77, 641–651. https://doi.org/10.1016/j.landusepol.2018.06.020.

Leitão, A.B., Ahern, J., 2002. Applying landscape ecological concepts and metrics in sustainable landscape planning. Landsc. Urban Plan. 59, 65–93. https://doi.org/10.1016/S0169-2046(02)00005-1.

Li, L., Zhu, A., Huang, L., Wang, Q., Chen, Y., Ooi, M.C.G., Wang, M., Wang, Y., Chan, A., 2022. Modeling the impacts of land use/land cover change on meteorology and air quality during 2000–2018 in the Yangtze River Delta region. China. Sci. Total Environ. 829, 154669. https://doi.org/10.1016/j.scitotenv.2022.154669.

Li, S., Lu, S., Xu, X., Zhao, N., Li, A., Xu, L., 2021. How human mega-events influence urban airborne PM2.5 pollution: a systematic review and meta-analysis. Environ. Pollut. 281, 117009. https://doi.org/10.1016/j.envpol.2021.117009.

Li, Xuecao, Gong, P., Zhou, Y., Wang, J., Bai, Y., Chen, B., Hu, T., Xiao, Y., Xu, B., Yang, J., Liu, X., Cai, W., Huang, H., Wu, T., Wang, X., Lin, P., Li, Xun, Chen, J., He, C., Li, Xia, Yu, L., Clinton, N., Zhu, Z., 2020. Mapping global urban boundaries from the global artificial impervious area (GAIA) data. Environ. Res. Lett. 15, 094044. https://doi.org/10.1088/1748-9326/ab9be3.

Li, Y., Zhang, Y.C., Wu, Q., Xue, R., Wang, X., Si, M., Zhang, Y.Y., 2023. Greening the concrete jungle: unveiling the co-mitigation of greenspace configuration on PM2.5 and land surface temperature with explanatory machine learning. URBAN For. URBAN Green. 88. https://doi.org/10.1016/j.ufug.2023.128086.

Liang, J., Gong, P., 2020. Urban and air pollution: a multi-city study of long-term effects of urban landscape patterns on air quality trends. Sci. Rep. 10, 1–13. https://doi.org/10.1038/s41598-020-74524-9.

Lin, J., Wei, K., Guan, Z., 2024. Exploring the connection between morphological characteristic of built-up areas and surface heat islands based on MSPA. Urban Clim. 53, 101764. https://doi.org/10.1016/j.uclim.2023.101764.

Lin, Y., Yuan, X., Zhai, T., Wang, J., 2020. Effects of land-use patterns on PM2.5 in China's developed coastal region: exploration and solutions. Sci. Total Environ. 703, 135602. https://doi.org/10.1016/j.scitotenv.2019.135602.

Liu, J., Yan, G., Wu, Y., Wang, Y., Zhang, Z., Zhang, M., 2018a. Wetlands with greater degree of urbanization improve PM2.5 removal efficiency. Chemosphere 207, 601–611. https://doi.org/10.1016/j.chemosphere.2018.05.131.

Liu, W., Holst, J., Yu, Z., 2014. Thresholds of landscape change: a new tool to manage green infrastructure and social–economic development. Landsc. Ecol. 29, 729–743. https://doi.org/10.1007/s10980-014-0007-1.

Liu, Y., Peng, J., Wang, Y., 2018b. Efficiency of landscape metrics characterizing urban land surface temperature. Landsc. Urban Plan. 180, 36–53. https://doi.org/10.1016/j.landurbplan.2018.08.006.

Liu, Y., Zhou, Y., 2021. Territory spatial planning and national governance system in China. Land Use Policy 102, 105288. https://doi.org/10.1016/j.landusepol.2021.105288.

Lu, D., Mao, W., Yang, D., Zhao, J., Xu, J., 2018. Effects of land use and landscape pattern on PM2.5 in Yangtze River Delta, China. Atmospheric Pollut. Res. 9, 705–713. https://doi.org/10.1016/j.apr.2018.01.012.

Lu, D., Xu, J., Yue, W., Mao, W., Yang, D., Wang, J., 2020. Response of PM2.5 pollution to land use in China. J. Clean. Prod. 244, 118741. https://doi.org/10.1016/j.jclepro.2019.118741.

Mo, Y., Kim, H.G., Huber, P.R., Thorne, J.H., Hijioka, Y., Lee, D.K., 2019. Influences of planning unit shape and size in landscapes dominated by different land-cover types on systematic conservation planning. Glob. Ecol. Conserv. 20, e00739. https://doi.org/10.1016/j.gecco.2019.e00739.

Ouyang, X., Shao, Q., Zhu, X., He, Q., Xiang, C., Wei, G., 2019. Environmental regulation, economic growth and air pollution: panel threshold analysis for OECD countries. Sci. Total Environ. 657, 234–241. https://doi.org/10.1016/j.scitotenv.2018.12.056.

Peng, J., Xie, P., Liu, Y., Ma, J., 2016. Urban thermal environment dynamics and associated landscape pattern factors: a case study in the Beijing metropolitan region. Remote Sens. Environ. 173, 145–155. https://doi.org/10.1016/j.rse.2015.11.027.

Qian, Z., Li, L., Lin, X., Sun, R., Chen, Y., 2024. Spatial and temporal variation of PM2.5 and the influence of vegetation in the Yangtze River Delta region. Atmospheric Pollut. Res. 15, 102266. https://doi.org/10.1016/j.apr.2024.102266.

Qu, Y., Wang, T., Yuan, C., Wu, H., Gao, L., Huang, C., Li, Y., Li, M., Xie, M., 2023. The underlying mechanisms of PM2.5 and O3 synergistic pollution in East China: photochemical and heterogeneous interactions. Sci. Total Environ. 873, 162434. https://doi.org/10.1016/j.scitotenv.2023.162434.

Ran, P., Hu, S., Frazier, A.E., Yang, S., Song, X., Qu, S., 2023. The dynamic relationships between landscape structure and ecosystem services: an empirical analysis from the Wuhan metropolitan area, China. J. Environ. Manage. 325, 116575. https://doi.org/10.1016/j.jenvman.2022.116575.

Ren, Y., Tang, X., Fan, T., Kang, D., 2023. Does the spatial pattern of urban blue–green space at city-level affects its cooling efficiency? Evidence from Yangtze River Economic Belt, China. Landsc. Ecol. Eng. 19, 363–379. https://doi.org/10.1007/s11355-023-00540-2.

Santiago, J.-L., Rivas, E., 2021. Advances on the influence of vegetation and forest on urban air quality and thermal comfort. Forests 12, 1133. https://doi.org/10.3390/f12081133.

Shen, Z., Zhang, Z., Cui, L., Xia, Z., Zhang, Y., 2023. Coordinated change of PM2.5 and multiple landscapes based on spatial coupling model: comparison of inland and waterfront cities. Environ. Impact Assess. Rev. 102, 107194. https://doi.org/10.1016/j.eiar.2023.107194.

Shih, W., 2017. Greenspace patterns and the mitigation of land surface temperature in Taipei metropolis. Habitat Int. 60, 69–80. https://doi.org/10.1016/j.habitatint.2016.12.006.

Silveira, C., Amaral, F.G., Dias, A.T.C., de Gois, G., Piston, N., 2024. The importance of private gardens and their spatial composition and configuration to urban heat island mitigation. Sustain. Cities Soc. 112. https://doi.org/10.1016/j.scs.2024.105589.

Taha, H., Wilkinson, J., Bornstein, R., Xiao, Q., McPherson, G., Simpson, J., Anderson, C., Lau, S., Lam, J., Blain, C., 2016. An urban-forest control measure for ozone in the Sacramento, CA Federal Non-Attainment Area (SFNA). Sustain. Cities Soc. 21, 51–65. https://doi.org/10.1016/j.scs.2015.11.004.

Tang, B., Wong, K.T., 2021. Threshold effects of incremental redevelopment of an industrial property on a residential neighbourhood. Landsc. Urban Plan. 208, 104037. https://doi.org/10.1016/j.landurbplan.2020.104037.

Teng, M., Zhou, Z., Wang, P., Xiao, W., Wu, C., Lord, E., 2016. Geotechnology-based modeling to optimize conservation of forest network in urban area. Environ. Manage. 57, 601–619. https://doi.org/10.1007/s00267-015-0642-6.

Tong, H., 1983. Threshold Models in Non-linear Time Series Analysis. Springer, New York, NY.

Vaz Monteiro, M., Doick, K.J., Handley, P., Peace, A., 2016. The impact of greenspace size on the extent of local nocturnal air temperature cooling in London. Urban For. Urban Green. 16, 160–169. https://doi.org/10.1016/j.ufug.2016.02.008.

Wang, C., Guo, M., Jin, J., Yang, Y., Ren, Y., Wang, Y., Cao, J., 2022a. Does the spatial pattern of plants and green space affect air pollutant concentrations? Evidence from 37 garden cities in China. Plants 11, 2847. https://doi.org/10.3390/plants11212847.

Wang, K., Ma, H., Fang, C., 2023a. The relationship evolution between urbanization and urban ecological resilience in the Northern Slope Economic Belt of Tianshan Mountains, China. Sustain. Cities Soc. 97, 104783. https://doi.org/10.1016/j.scs.2023.104783.

Wang, L., Qin, K., Zhao, B., 2024a. Spatiotemporal variations in the association between PM2.5 and ozone in the yangtze river economic belt: impacts of meteorological and emissions factors. Atmos. Environ. 329, 120534. https://doi.org/10.1016/j.atmosenv.2024.120534.

Wang, M., Wu, Y., Wang, Y., Hu, P., Sun, G., 2023b. Exploration of spatial heterogeneity in the effect of woodland proportion on PM2.5: an empirical study from the Yangtze River economic Belt, China. Atmospheric Pollut. Res. 14, 101914. https://doi.org/10.1016/j.apr.2023.101914.

Wang, P., Zeng, C., Zhang, W., Lv, T., Miao, X., Xiang, H., 2024b. Investigation of the spatial effects on PM2.5 in relation to land use and ecological restoration in urban agglomerations. Sci. Total Environ. 913, 169665. https://doi.org/10.1016/j.scitotenv.2023.169665.

Wang, Q., Wang, X., Li, R., 2022b. Does urbanization redefine the environmental Kuznets curve? An empirical analysis of 134 Countries. Sustain. Cities Soc. 76, 103382. https://doi.org/10.1016/j.scs.2021.103382.

Wang, Q., Wang, X., Liu, Y., Li, R., 2021. Urbanization and water consumption at national- and subnational-scale: the roles of structural changes in economy, population, and resources. Sustain. Cities Soc. 75, 103272. https://doi.org/10.1016/j.scs.2021.103272.

Wang, X., Tian, G., Yang, D., Zhang, W., Lu, D., Liu, Z., 2018. Responses of PM2.5 pollution to urbanization in China. Energy Policy 123, 602–610. https://doi.org/10.1016/j.enpol.2018.09.001.

Wang, Y., Dawson, R., Han, D., Peng, J., Liu, Z., Ding, Y., 2001. Landscape ecological planning and design of degraded mining land. Land Degrad. Dev. 12, 449–459. https://doi.org/10.1002/ldr.462.

Wang, Y., Wang, M., Wu, Y., Sun, G., 2023c. Exploring the effect of ecological land structure on PM2.5: a panel data study based on 277 prefecture-level cities in China. Environ. Int. 174, 107889. https://doi.org/10.1016/j.envint.2023.107889.

Wei, J., Li, Z., Li, K., Dickerson, R.R., Pinker, R.T., Wang, J., Liu, X., Sun, L., Xue, W., Cribb, M., 2022. Full-coverage mapping and spatiotemporal variations of ground-level ozone (O3) pollution from 2013 to 2020 across China. Remote Sens. Environ. 270, 112775. https://doi.org/10.1016/j.rse.2021.112775.

Wei, J., Li, Z., Lyapustin, A., Sun, L., Peng, Y., Xue, W., Su, T., Cribb, M., 2021. Reconstructing 1-km-resolution high-quality PM2.5 data records from 2000 to 2018 in China: spatiotemporal variations and policy implications. Remote Sens. Environ. 252, 112136. https://doi.org/10.1016/j.rse.2020.112136.

Wu, H., Guo, B., Guo, T., Pei, L., Jing, P., Wang, Y., Ma, X., Bai, H., Wang, Z., Xie, T., Chen, M., 2024. A study on identifying synergistic prevention and control regions for PM2.5 and O3 and exploring their spatiotemporal dynamic in China. Environ. Pollut. 341, 122880. https://doi.org/10.1016/j.envpol.2023.122880.

Wu, J., Wang, Y., Liang, J., Yao, F., 2021. Exploring common factors influencing PM2.5 and O3 concentrations in the Pearl River Delta: tradeoffs and synergies. Environ. Pollut. 285, 117138. https://doi.org/10.1016/j.envpol.2021.117138.

Xie, Y., Ying, J., Zou, J., Li, R., Zhang, H., Shi, Q., Li, Y., 2024. Habitat protection in urban–rural fringes through coordinated ecological network construction and territorial planning. Land 13, 935. https://doi.org/10.3390/land13070935.

Yang, H., Leng, Q., Xiao, Y., Chen, W., 2022. Investigating the impact of urban landscape composition and configuration on PM2.5 concentration under the LCZ scheme: a case study in Nanchang, China. Sustain. Cities Soc. 84, 104006. https://doi.org/10.1016/j.scs.2022.104006.

Yang, J., Chen, X., Li, M., Yao, Q., Lv, Q., Gao, B., Chen, Z., 2023. The division of PM2.5-O3 composite airborne pollution across China based on spatiotemporal clustering. J. Clean. Prod. 401, 136706. https://doi.org/10.1016/j.jclepro.2023.136706.

Yang, J., Huang, X., 2023. The 30 m annual land cover datasets and its dynamics in China from 1985 to 2022. https://doi.org/10.5281/zenodo.8176941.

Yao, F., Zhu, H., Wang, M., 2021. The impact of multiple dimensions of urbanization on CO2 emissions: a spatial and threshold analysis of panel data on China's prefecture-level cities. Sustain. Cities Soc. 73, 103113. https://doi.org/10.1016/j.scs.2021.103113.

Yu, Q., Li, Z., Zhao, W., Zhang, G., Xiong, X., Wu, Z., 2024. Modeling and control strategy optimizing of solar flux distribution in a four quadrant and adjustable focusing solar furnace. Appl. Energy 363, 123121. https://doi.org/10.1016/j.apenergy.2024.123121.

Yu, Z., Xiao, L., Chen, X., He, Z., Guo, Q., Vejre, H., 2018. Spatial restructuring and land consolidation of urban-rural settlement in mountainous areas based on ecological niche perspective. J. Geogr. Sci. 28, 131–151. https://doi.org/10.1007/s11442-018-1464-2.

Yu, Z., Yang, G., Zuo, S., Jørgensen, G., Koga, M., Vejre, H., 2020. Critical review on the cooling effect of urban blue-green space: a threshold-size perspective. Urban For. Urban Green. 49, 126630. https://doi.org/10.1016/j.ufug.2020.126630.

Zhang, R., Chen, G., Yin, Z., Zhang, Y., Ma, K., 2021. Urban greening based on the supply and demand of atmospheric PM2.5 removal. Ecol. Indic. 126, 107696. https://doi.org/10.1016/j.ecolind.2021.107696.

Zhang, X., Cheng, C., Zhao, H., 2022. A health impact and economic loss assessment of O3 and PM2.5 exposure in China from 2015 to 2020. GeoHealth 6, e2021GH000531. https://doi.org/10.1029/2021GH000531.

Zhang, X., Fan, H., Hou, H., Xu, C., Sun, L., Li, Q., 2024. Spatiotemporal evolution and multi-scale coupling effects of land-use carbon emissions and ecological environmental quality. Sci. Total Environ. 922, 171149. https://doi.org/10.1016/j.scitotenv.2024.171149.

Zhao, M., Zhang, Y., 2024. Exploring the dose-response of landscape preference: a case study in Singapore. Appl. Geogr. 170, 103357. https://doi.org/10.1016/j.apgeog.2024.103357.

Zhao, X., Xu, Y., Pu, J., Tao, J., Chen, Y., Huang, P., Shi, X., Ran, Y., Gu, Z., 2024. Achieving the supply-demand balance of ecosystem services through zoning regulation based on land use thresholds. Land Use Policy 139, 107056. https://doi.org/10.1016/j.landusepol.2024.107056.

Zheng, L., Huang, H., Zhang, X., 2023. Human capital and livelihood resilience of farmers in poverty alleviated areas-A threshold regression model test. J. Arid Land Resour. Environ. Times 37, 69–75. https://doi.org/10.13448/j.cnki.jalre.2023.114.

Zhou, M., He, Y., Li, Y., Wang, J., Yao, S., 2024. Construction of ecological security pattern of Jiangnan water town considering water-related ecosystem services: a case study of Yuecheng District, Shaoxing. Geocarto Int 39, 2417872. https://doi.org/10.1080/10106049.2024.2417872.

Zhou, X., Zhang, S., Zhu, D., 2021. Impact of urban water networks on microclimate and PM2.5 distribution in downtown areas: a case study of wuhan. Build. Environ. 203, 108073. https://doi.org/10.1016/j.buildenv.2021.108073.

Zhou, Y., Liu, H., Zhou, J., Xia, M., 2019. GIS-based urban afforestation spatial patterns and a strategy for PM2.5 removal. Forests 10, 875. https://doi.org/10.3390/f10100875.

Zhu, C., Zeng, Y., 2018. Effects of urban lake wetlands on the spatial and temporal distribution of air PM10 and PM2.5 in the spring in Wuhan. Urban For. Urban Green. 31, 142–156. https://doi.org/10.1016/j.ufug.2018.02.008.

Zhu, H., Zhang, P., Wang, N., Zhang, F., Ma, W., Wen, F., Li, M., Wang, Y., Fan, X., Hou, K., Han, Y., 2024. Investigating the multiscale associations between urban landscape patterns and PM1 pollution in China using a new combined framework. J. Clean. Prod. 456. https://doi.org/10.1016/j.jclepro.2024.142306.